Evaluation of Sr$_2$MMoO$_6$ (M = Mg, Mn) as anode materials in solid-oxide fuel cells: A neutron diffraction study

L. Troncoso,[1,a] M. J. Martínez-Lope,[2] J. A. Alonso,[2] and M. T. Fernández-Díaz[3]

[1]*Departamento de Física, Facultad de Ciencias, Universidad de Santiago de Chile, Av. Lib. Bernardo O'Higgins 3363, Santiago, Chile*
[2]*Instituto de Ciencia de Materiales, CSIC, Cantoblanco, 28049 Madrid, Spain*
[3]*Institut Laue-Langevin, B.P. 156, F-38042 Grenoble Cedex 9, France*

Sr$_2$MMoO$_6$ (M = Mg, Mn) double perovskites have recently been proposed as anode materials in solid-oxide fuel cells (SOFC). The evolution of their crystal structures has been followed by "*in situ*" temperature-dependent neutron powder diffraction from 25 °C room temperature (RT) to 930 °C by heating in ultrahigh vacuum (P$_{O2}$ ≈ 10^{-6} Torr) in order to simulate the reducing atmosphere corresponding to the working conditions of an anode in a SOFC. At RT, the samples are described as tetragonal (I4/m space group) and monoclinic (P2$_1$/n) for M = Mg, Mn, respectively. Sr$_2$MgMoO$_6$ undergoes a structural phase transition from tetragonal to cubic (Fm-3m) below 300 °C; Sr$_2$MnMoO$_6$ experiences two consecutive phase transitions to tetragonal (I4/m) and finally cubic (Fm-3m) at 600 °C and above. In the cubic phases, the absence of octahedral tilting accounts for a good overlap between the oxygen and transition-metal orbitals, resulting in a good electronic conductivity; a high mobility of the oxygen atoms is derived from the elevated displacement parameters, for instance 3.0 Å^2 and 4.6 Å^2 at 930 °C for M = Mg, Mn, respectively. Both factors contribute to the excellent performance described for these mixed ionic and electronic conductor oxides as anodes in single fuel cells. From dilatometric measurements, the thermal expansion coefficients (TEC) in the cubic region are 12.7 × 10^{-6} K^{-1} and 13.0 × 10^{-6} K^{-1} for M = Mg and Mn, respectively. These figures are comparable to those obtained from the mentioned structural analysis; moreover, the TECs for the cubic phases perfectly match those of the usual electrolytes in a SOFC. © *2013 American Institute of Physics*. [http://dx.doi.org/10.1063/1.4774764]

INTRODUCTION

Many efforts are being devoted to design and prepare anode materials for solid-oxide fuel cells (SOFC) able to perform at intermediate temperatures (550-850 °C), motivated by the purpose of decreasing the operation cost. A necessary requirement for a material to perform well as an SOFC anode in such conditions is that it is a "mixed ionic and electronic conductor" (MIEC). It must also have a thermal-expansion coefficient that is compatible with that of the solid oxide electrolyte. ABO$_3$ perovskites exhibit a well-known ability to accommodate a wide range of oxygen deficiency, giving good oxide ion conduction and mixed oxidation states of B-site transition metal, resulting in good electronic conduction.[1,2] Double perovskite A$_2$BB'O$_6$ oxides contain two different B and B' cations, exhibiting 1:1 long range ordering; typically A are alkaline-earth or rare-earth ions and B and B' transition metal ions. The crystallographic structure of these oxides can be cubic, orthorhombic, or monoclinic, depending on the occurrence of octahedral tilting.[3] Double perovskites have been proposed as good anode materials in SOFC with better fuel flexibility than the usual metal-electrolyte cermets.[4] In particular, the double-perovskite oxides Sr$_2$MMoO$_6$ (M = Mg, Mn) have been recently shown to pro-

vide a stable performance as anode of a SOFC operating on H$_2$ as fuel and a promising performance with CH$_4$ as fuel.[5]

In the present work, we are interested in evaluating the structural reasons for such a good performance. We have investigated the thermal evolution of the crystal structure of Sr$_2$MMoO$_6$ (M = Mg, Mn) in the actual working conditions of an anode in a SOFC from "*in situ*" neutron powder diffraction (NPD) experiments, in complement with thermal expansion measurements under reducing atmosphere.
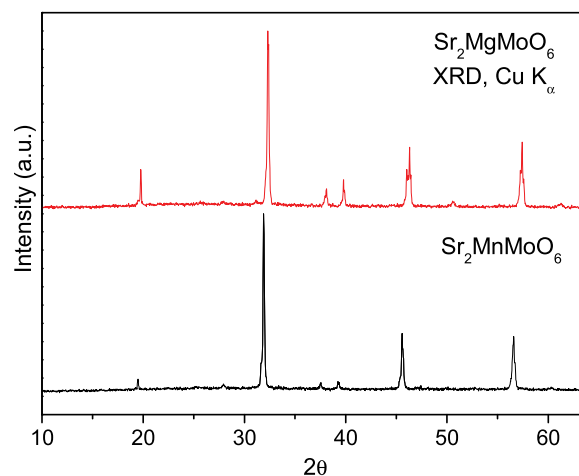
FIG. 1. XRD patterns of Sr$_2$MMoO$_6$ (M = Mg, Mn).

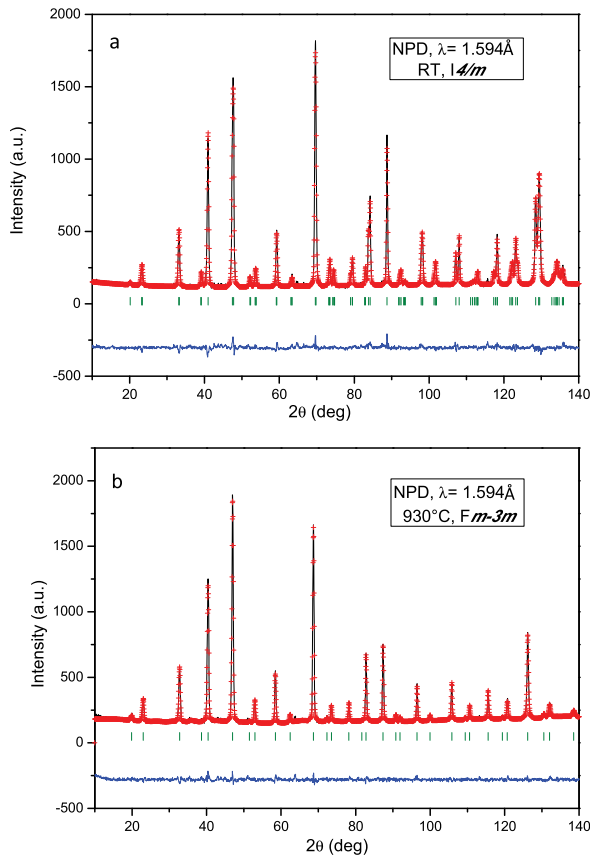a)Author to whom correspondence should be addressed. Electronic mail: Loreto.troncoso@usach.cl.

FIG. 2. Observed (crosses), calculated (full line), and difference (at the bottom) NPD profiles for $Sr_2MgMoO_{6-\delta}$ at (a) 25 °C refined in the tetragonal $I4/m$ space group and (b) 930 °C, refined in the cubic $Fm\text{-}3m$ space group. The vertical markers correspond to the allowed Bragg reflections.

EXPERIMENTAL

The stoichiometric Sr_2MMoO_6 (M = Mg, Mn) oxides were prepared via a nitrate-citrate route. The starting materials $Sr(NO_3)_2$, $(NH_4)_6Mo_7O_{24}\cdot 4H_2O$, and MgO or $MnCO_3$ of analytical grade were dissolved under stirring in 250 ml of 10% citric-acid aqueous with several droplets of concentrated HNO_3. The mixture of citrate and nitrate solutions was slowly evaporated, leading to organic resins where a random distribution of the involved cations is expected at an atomic level. The resin was dried at 120 °C and slowly decomposed at temperatures up to 600 °C. A subsequent treatment at 800 °C for 2 h ensures the total elimination of all the organic materials and nitrates. For M = Mn, the resulting highly reactive precursors were heated at 1000 °C for 12 h in air followed by a reducing treatment at 1000 °C for 8 h in a 15% H_2-85% N_2 flow. For M = Mg, the precursor powders were heated at 1150 °C in air followed by a thermal treatment at 1200 °C for 12 h in a 5% H_2-95% N_2 flow.

The reaction products were characterized by x-ray diffraction (XRD) for phase identification and to asses phase purity. The characterization was performed with a Bruker-axs D8 diffractometer (40 kV, 30 mA) in Bragg-Brentano reflection geometry with Cu Kα_1 ($\lambda = 1.5406$ Å) and Cu Kα_2 ($\lambda = 1.5444$ Å) radiation. NPD data were collected in the D2B diffractometer at the Institut Laue-Langevin, Grenoble, in the high-resolution configuration with a neutron wavelength $\lambda = 1.549$ Å. About 2 g of the sample was contained in a vanadium can and placed in the isothermal zone of a furnace with a vanadium resistor operating under vacuum ($P_{O_2} \approx 10^{-6}$ Torr). The measurements were carried out at 25, 300,

TABLE I. Structural parameters for Sr_2MgMoO_6 from *in situ* NPD data at different temperatures. The bold characters indicate the symmetry equivalent positions.

T (°C)	25	300	600	800	930
Space group	I 4/m	Fm-3m	Fm-3m	Fm-3m	Fm-3m
a (Å)	5.5712(1)	7.9252(1)	7.9569(1)	7.9788(1)	7.9936(2)
b (Å)	5.5712(1)	a	a	a	a
c (Å)	7.9234(2)	a	a	a	a
V (Å³)	245.93 (0.8)	497.77(1)	503.76(2)	507.94(2)	510.77(2)
Sr	**4d (0 1/2 1/4)**	**8c (1/4,1/4,1/4)**	**8c (1/4,1/4,1/4)**	**8c (1/4,1/4,1/4)**	**8c (1/4,1/4,1/4)**
B_{iso} (Å²)	0.47(5)	1.37	2.00	2.45	2.73
Mg	**2a (0 0 0)**	**4a (0 0 0)**	**4a (0 0 0)**	**4a (0 0 0)**	**4a (0 0 0)**
B_{iso} (Å²)	0.24(4)	0.80(3)	1.25(2)	1.37(2)	1.70(3)
F_{occ} (Mg/Mo)		0.87(7)/0.13(7)	0.79(7)/0.21(7)	0.91(6)/0.09(6)	0.84(7)/0.16(7)
Mo	**2b (0 0 1/2)**	**4b(1/2,0,0)**	**4b(1/2,0,0)**	**4b(1/2,0,0)**	**4b(1/2,0,0)**
B_{iso} (Å²)	0.16(3)	0.50(2)	0.72(2)	1.00(2)	1.17(2)
F_{occ} Mo/Mg		0.13(7)/0.87(7)	0.21(7)/0.79(7)	0.13(6)/0.87(6)	0.09(7)/0.91(7)
O1	**4e (0 0 z)**	**24e (x,0,0)**	**24e (x,0,0)**	**24e (x,0,0)**	**24e (x,0,0)**
x	0	0.2594(2)	0.2599(2)	0.2603(3)	0.2605(3)
z	0.2595(8)	0	0	0	0
B_{eq} (Å²)	0.49	1.68	2.27	2.67	3.02
O2	**8h (x y 0)**				
x	0.2830(7)	…	…	…	…
y	0.2303(6)	…	…	…	…
B_{eq} (Å²)	0.6710				
Reliability factors					
χ^2	2.07	2.02	1.87	1.51	1.56
R_p (%)	3.92	3.40	3.45	3.16	3.22
R_{wp} (%)	5.02	4.42	4.47	4.04	4.10
R_{Bragg} (%)	4.86	2.42	2.54	2.58	2.98

TABLE II. Anisotropic factors for Sr_2MgMoO_6 from *in situ* NPD data at different temperatures.

T (°C)	25	300	600	800	930
O1					
β_{11}	0.0054(6)	0.0019(2)	0.0027(3)	0.0038(3)	0.0046(3)
β_{22}	0.0054(6)	0.0091(2)	0.0121(2)	0.0138(2)	0.0154(2)
β_{33}	0.0006(5)	0.0091(2)	0.0121(2)	0.0138(2)	0.0154(2)
O2					
β_{11}	0.0064(14)				
β_{22}	0.0016(15)				
β_{33}	0.0040(3)				

600, 800, and 930 °C for M = Mg; and 25, 200, 400, 600, 800, and 930 °C for M = Mn. The counting time for each pattern was 2 h. The diffraction data were analysed by the Rietveld method[6] with the FULLPROF program.[7] The line shape of the diffraction peaks was generated by a pseudo-Voigt function. The following parameters were refined: background points, zero shift, half width, pseudo-Voigt, scale factor, and unit-cell parameters. Positional factors for oxygen atoms and anisotropic displacement factors were also refined for the NPD data. The coherent scattering lengths for Sr, Mg, Mn, Mo, and O were 7.02, 2.49, −3.73, 6.715, and 5.803 fm, respectively.

For the thermal expansion measurements of Sr_2MMoO_6 (M = Mg, Mn), the powders were uniaxially pressed (~1 ton) into a cylindrical pellet sintered at 1000 °C for 6 h in 5% H_2/95% N_2 atmosphere and at 1000 °C for 6 h in 15% H_2/85% N_2, respectively. The thermal expansion was determined by dilatometric analysis using a Linseis L75H1000 dilatometer under a 5% H_2/N_2 flow. Both pellet were densified up to 90%–95% and polished to obtain a thickness as uniform as possible. The densities of the pellets were determined using the following equations:
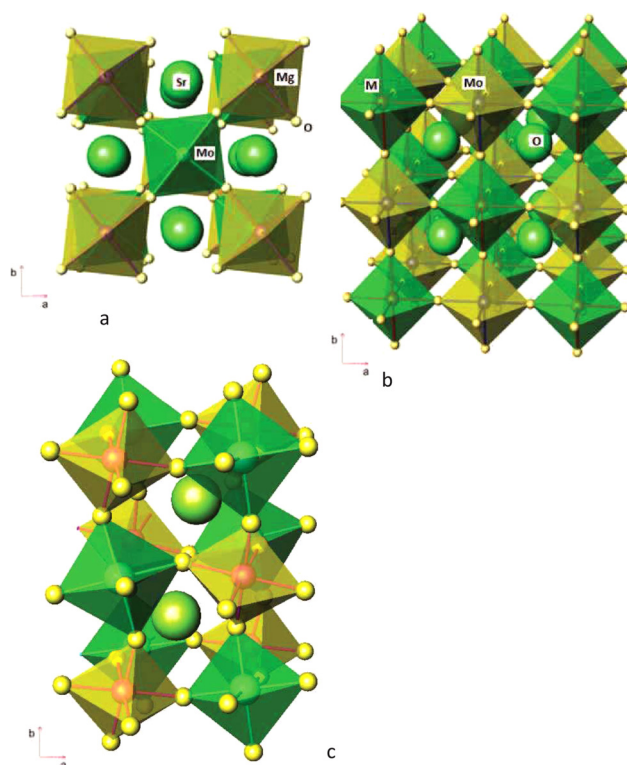
$$\varphi = \frac{m}{V} \quad (1)$$

and

$$\varphi_x = \frac{Z \cdot W}{V \cdot N_{avog}}, \quad (2)$$

FIG. 3. Schematic representation of the crystal structure of (a) tetragonal Sr_2MMoO_6, approximately projected along the [001] direction, showing the antiphase tilting of the MO_6 and MoO_6 octahedra; (b) cubic phase, showing the untilted, alternating MO_6 and MoO_6 octahedra; (c) monoclinic structure of Sr_2MnMoO_6, highlighting the tilting of the MnO_6 and MoO_6 octahedra.

where φ and φ_x are the experimental and theoretical densities of the sample, respectively.

The percentage of the degree of densification for the pellets is obtained as $(\varphi/\varphi_x) \times 100$.

RESULTS AND DISCUSSION

Sr_2MMoO_6 (M = Mg, Mn) were obtained as black, well-crystallized powders. No impurity phases were detected. The laboratory XRD diagrams at room temperature (RT) of both perovskites are shown in Fig. 1.

TABLE III. Interatomic distances (Å) and angles (°) for tetragonal and cubic Sr_2MgMoO_6 at increasing temperatures. The bold characters indicate the average atomic differences.

T (°C)	25	T (°C)	300	600	800	930
Mg–O1 (x2)	2.056(6)	Mg–O1 (x12)	2.056(2)	2.068(2)	2.076(2)	2.082(2)
Mg–O2 (x4)	2.033(4)					
⟨Mg–O⟩	2.045(5)	**⟨Mg–O⟩**	2.056(2)	2.068(2)	2.076(2)	2.082(2)
Mo–O1 (x2)	1.906(6)	Mo–O1 (x6)	1.907(2)	1.910(2)	1.913(2)	1.914(2)
Mo–O2 (x4)	1.929(4)					
⟨Mo–O⟩	1.918(5)	**⟨Mo–O⟩**	1.907(2)	1.910(2)	1.913(2)	1.914(2)
Sr–O1 (x4)	2.787(2)	Sr–O1 (x6)	2.803(5)	2.814(6)	2.822(8)	2.827(8)
Sr–O2 (x4)	2.944(3)					
Sr–O2 (x4)	2.652(2)					
⟨Sr–O⟩	2.794(3)	**⟨Sr–O⟩**	2.803(5)	2.814(6)	2.822(8)	2.827(8)
Mg–O1–Mo	180(3)	**Mg–O1–Mo**	180.0	180.0	180.0	180.0
Mg–O2–Mo	167.96(15)					

Sr_2MgMoO_6

At RT, the crystal structure was refined from NPD data as a tetragonal double perovskite defined in the $I4/m$ group (No. 87) with a $= 5.5712(1)$ Å and c $= 7.9234(2)$ Å, in agreement with previous reports.[8] For the tetragonal structure, Sr atoms were located at 4d positions, Mg at 2a, Mo at 2b, and oxygen atoms at 4e and 8h sites. Fig. 2(a) shows the quality of the fit at RT. Table I contains the main atomic parameters after the refinement, Table II lists the anisotropic thermal factors and Table III lists the main interatomic distances and angles. A view of the tetragonal crystal structure is shown in Fig. 3(a). It contains alternating MgO_6 and MoO_6 octahedra, tilted in anti-phase by 6.05°. This corresponds to the $a^0a^0c^-$ tilting system (Glazer's notation) derived by Woodward for 1:1 ordering of double perovskites,[9] consistent with space group I4/m.

A structural transition from tetragonal to cubic symmetry is observed, occurring between 25 and 300 °C. In the 300–930 °C temperature range, the crystal structure for Sr_2MgMoO_6 was successfully refined in the $Fm\text{-}3m$ space group (No. 225). This is a double perovskite structure characterized by the long-range 1:1 ordering the Mg and Mo over the B sites of the perovskite structure, with doubled unit-cell parameter with respect to the arystotype a_0, as a $= 2xa_0$. In this structure, Sr atoms are located at the 8c positions, Mg and Mo are placed at the 4a and 4b sites, respectively, and the oxygen atoms occupy the 24e positions. The antisite disordering, assuming that some Mg occupies the Mo sites and vice-versa was also refined. The refinement of the oxygen occupancy factors did not lead to a significant oxygen deficiency within the standard deviations in all the temperature range. Fig. 2(b) illustrates the goodness of the fit

TABLE IV. Structural parameters for Sr_2MnMoO_6 from *in situ* NPD data at different temperatures. The bold characters indicate the symmetry equivalent positions.

T (°C)	25	200	400	600	800	930
Space group	$P2_1/n$	$P2_1/n$	$I4/m$	$Fm\text{-}3m$	$Fm\text{-}3m$	$Fm\text{-}3m$
a (Å)	5.6671(2)	5.6859(5)	5.6790(3)	8.0610(2)	8.0821(3)	8.0954(3)
b (Å)	5.6538(1)	5.6642(4)	5.6790(3)	a	a	A
c (Å)	7.9968(2)	8.0104(6)	8.0602(6)	a	a	A
α (°)	90	90	90	90	90	90
β (°)	89.93(3)	89.96(4)	α	α	α	α
γ (°)	α	90	α	α	α	α
Volume (Å^3)	256.22(1)	257.99(4)	259.96(3)	523.80(3)	527.93(3)	530.54(3)
Atoms						
Sr	**4e (x y z)**	**4e (x y z)**	**4d (0 1/2 1/4)**	**8c (1/4 1/4 1/4)**	**8c (1/4 1/4 1/4)**	**8c (1/4 1/4 1/4)**
x	0.997(1)	1.026(4)	0	0.25	0.25	0.25
y	0.019(1)	0.002 (3)	0.5	x	x	X
z	0.249(1)	0.248(2)	0.25	x	x	X
B_{eq} (Å^2)	1.10	1.88	2.29(2)	2.98	3.37	3.80
Mn	**2d (1/2 0 0)**	**2d (1/2 0 0)**	**2a (0 0 0)**	**4a (0 0 0)**	**4a (0 0 0)**	**4a (0 0 0)**
F_{occ} (Mn/Mo)				0.96(5)/0.04(5)	0.96(5)/0.04(5)	0.96(5)/0.04(5)
B_{eq} (Å^2)	1.24	0.86	1.30(5)	1.72(3)	1.71(3)	2.09(3)
Mo	**2c (1/2 0 1/2)**	**2c (1/2 0 1/2)**	**2b (0 0 1/2)**	**4b (1/2 0 0)**	**4b (1/2 0 0)**	**4b (1/2 0 0)**
F_{occ} (Mo/Mn)				0.04(5)/0.96(5)	0.04(5)/0.96(5)	0.04(5)/0.96(5)
B_{eq} (Å^2)	0.51	0.73	1.17(2)	1.37(2)	1.50(1)	1.56(2)
O1	**4e (x y z)**	**4e (x y z)**	**4e (0 0 Z)**	**24e (x 0 0)**	**24e (x 0 0)**	**24e (x 0 0)**
x	0.054(1)	0.031(5)	0	0.264(3)	0.264(3)	0.264(3)
y	0.493(1)	0.499(4)	0	0	0	0
z	0.237(1)	0.235(2)	0.264(1)	0	0	0
B_{eq} (Å^2)	0.64	3.19	3.70	4.14	4.53	4.63
O2	**4e (x y z)**	**4e (x y z)**	**8h (x y 0)**			
x	0.737(1)	0.732(3)	0.289(1)			
y	0.290(1)	0.268(3)	0.238(1)			
z	0.028(1)	0.019(2)	0.000(1)			
B_{eq} (Å^2)	1.08	4.22	3.36			
O3	**4e (x y z)**	**4e (x y z)**				
x	0.207(1)	0.222(2)				
y	0.234(1)	0.252(3)				
z	0.973(1)	0.969(2)				
B_{eq} (Å^2)	0.94	2.89				
Reliability factors						
χ^2	1.33	1.17	1.28	1.32	1.32	1.51
R_p (%)	3.91	2.77	2.85	2.90	2.92	2.97
R_{wp} (%)	4.99	3.49	3.61	3.67	3.66	3.85
R_{Bragg} (%)	4.15	3.91	3.46	3.74	3.56	4.25

of the cubic phase at 930 °C for this double perovskite, and Fig. 3(b) displays a schematic view of the cubic $2a_0$ structure, showing the untilted, alternating MgO_6 and MoO_6 octahedra.

Sr$_2$MnMoO$_6$

At RT, the crystal structure has been Rietveld-refined in the monoclinic P2$_1$/n space group (No. 14) with a = 5.6671(1) Å, b = 5.6537(1) Å, and c = 7.9969(2) Å, in agreement with previous reports.[3] In this model, Sr, O1, O2, and O3 atoms are located at 4e positions, Mn at 2d and Mo at 2c sites. Table IV lists the main atomic parameters after the refinement and Table V the anisotropic displacement factors. Fig. 4(a) shows the quality of the fit at RT. A view of the monoclinic crystal structure is shown in Fig. 3(c). It contains alternating MnO_6 and MoO_6 octahedral, tilted by 8.9°, 8.8°, and 9.3° along the three pseudocubic axis, according to the tilting scheme $a^- b^+ c^-$ as derived by Woodward for long-range ordered P2$_1$/n double perovskites.[9]

At 200 °C, the structure remains monoclinic. Between 200 and 400 °C, there is a phase transition to a tetragonal structure, with the appearance of a characteristic splitting of some high-angle peaks, as shown in the inset of Fig. 4(a). At 400 °C, the crystal structure can be refined in the same tetragonal model described in the I4/m space group for M = Mg. The MnO_6 and MoO_6 octahedra are tilted in anti-phase by 5.8°. Finally, at 600 °C, the mentioned splitting disappears as the sample becomes cubic (space group Fm-3m), as shown in the inset of Fig. 4(b); the 800 and 930 °C data were also fitted in the cubic structure. As observed for M = Mg, there is no deviation from the full oxygen stoichiometry in all the temperature range. Figures 4(a) and 4(b) illustrate the quality of the refinement. Table VI summarizes the main interatomic distances and angles from RT to 930 °C of the perovskite structure.

The equivalent isotropic displacement factors of the oxygen atoms in the cubic phase increase for both structures, suggesting an elevated ionic mobility of oxide ions especially at high temperatures T > 300 °C (Fig. 5).

Thermal expansion

From the thermal variation of the unit-cell parameters, we have estimated the thermal expansion coefficients (TEC) using the following equation:

$$TEC = (a_{Tf} - a_{Ti}/a_{Ti})/T_f - T_i. \qquad (3)$$

In the high-temperature region where the cubic Fm-3m phase is stable, a TEC of 13.5×10^{-6} K^{-1} was obtained between $T_i = 300$ °C and $T_f = 930$ °C for Sr$_2$MgMoO$_6$. For Sr$_2$MnMoO$_6$, the TEC obtained was 12.8×10^{-6} K^{-1} between $T_i = 600$ °C and $T_f = 930$ °C.

Alternatively, the TECs were determined by dilatometric analysis. The measurement of TECs was carried out on densified samples to avoid the contraction effect that would be observed upon the densification process at high temperatures. Both samples were cycled between 35 and 900 °C for several times; the data were only recorded during the heating runs. Fig. 6 shows no abrupt changes in thermal expansion; the tetragonal to cubic phase transition is probably too subtle to give rise to a significant change of slope in the corresponding temperature range. Therefore, the absence of abrupt changes makes both materials suitable as electrodes in SOFC, from this point of view. The average TEC obtained from both curves are 12.7×10^{-6} K^{-1} and 13.0×10^{-6} K^{-1} for M = Mg and Mn, respectively, in good agreement with

TABLE V. Anisotropic factors for Sr$_2$MnMoO$_6$ from *in situ* NPD data at different temperatures.

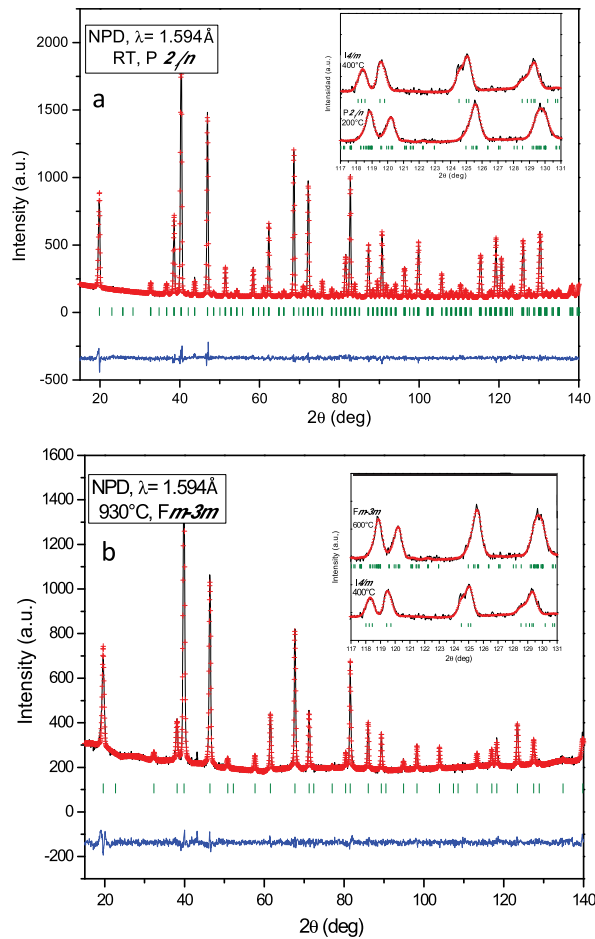| T (°C)	RT	200	T(°C)	RT	200	400	600	800	930
Sr			**O1**						
β_{11}	0.006(1)	0.009(2)	β_{11}	0.009(2)	0.055(1)	0.037(3)	0.005(5)	0.006 (5)	0.007(5)
β_{22}	0.010(1)	0.020(4)	β_{22}	0.005(2)	0.019(6)	0.037(3)	0.022(4)	0.023(4)	0.023(4)
β_{33}	0.005(1)	0.007(4)	β_{33}	0.001(1)	0.001(2)	0.007(1)	0.022(4)	0.023(4)	0.023(4)
β_{12}	−0.002(1)	−0.001(3)	β_{12}	0.000(1)	0.003(7)				
β_{13}	−0.000(1)	0.001(3)	β_{13}	−0.001(9)	−0.005(3)				
β_{23}	0.001(1)	0.003(3)	β_{23}	0.001(1)	0.009(3)				
Mn			**O2**						
β_{11}	0.010(5)	0.001(5)	β_{11}	0.006(1)	0.064(8)	0.021(2)			
β_{22}	0.003(4)	0.006(6)	β_{22}	0.007(1)	0.018(6)	0.015(3)			
β_{33}	0.008(3)	0.006(4)	β_{33}	0.006(1)	0.008(3)	0.021(1)			
β_{12}	0.000(1)	0.001(6)	β_{12}	−0.002(1)	0.011(6)	−0.009(2)			
β_{13}	−0.007(4)	−0.004(7)	β_{13}	0.001(8)	0.007(4)	0.000(1)			
β_{23}	−0.001(2)	0.008(5)	β_{23}	0.003(1)	0.007(5)	0.000(1)			
Mo			**O3**						
β_{11}	0.003(2)	0.006(3)	β_{11}	0.009(1)	0.013(3)				
β_{22}	0.005(2)	0.005(3)	β_{22}	0.010(2)	0.037(7)				
β_{33}	0.002(1)	0.003(2)	β_{12}	0.002(1)	0.009(3)				
β_{12}	−0.002(2)	0.001(3)	β_{12}	0.005(2)	0.023(4)				
β_{13}	0.002(2)	−0.005(5)	β_{13}	−0.002(1)	0.001(2)				
β_{23}	0.002(1)	−0.002(2)	β_{23}	−0.002(1)	0.002(5)				

FIG. 4. Observed (crosses), calculated (full line), and difference (at the bottom) NPD profiles for Sr₂MnMoO₆ at (a) 25 °C, refined in P2₁/n, (b) 930 °C refined in the cubic F*m-3m* space group. The vertical markers correspond to the allowed Bragg reflections. The insets show high-angle regions highlighting the evolution of some superstructure reflection.

those determined from NPD data. The thermal expansion coefficients of the anode must be compatible with that of the solid electrolyte in order to prevent the fracture of the SOFC during fuel cell operation cycles.[10] Typical values for the electrolyte are between 11.4×10^{-6} and 12.1×10^{-6} K⁻¹,[11,12] similar to those observed for the present materials.

A last issue is that concerning the full oxygen stoichiometry determined by neutron diffraction for both perovskite oxides. In principle, it is believed that the ionic transport, required for the performance of the anode materials, works with a vacancy mechanism, the pre-existing vacancies being filled by neighboring oxygen atoms. However, in this case the neutron data consistently indicate, for both compounds at all the measured temperatures, that the perovskites are strictly oxygen stoichiometric. This behavior has been observed before in other double perovskite oxides, also used as anodes in SOFC.[13] As it is certain that all these materials combine an excellent electronic conductivity with a sufficient ionic transport of oxide anions, we could imagine a mechanism where surface oxygen atoms in contact with the fuel (typically H₂) are removed to give H₂O, and the created vacancies (in the surface) are instantaneously filled by internal oxygen, the vacancies diffusing across the bulk, finally reaching the electrolyte where they are recombined with O^{2-} ions. In other words, these double perovskites do not contain a measurable concentration of permanent vacancies, but the lability of the oxygen atoms is sufficiently high to ensure an ionic transport from the surface to the electrolyte, via transient vacancies. Such a mechanism is possible in the present Mo-containing perovskites since, as noted by Goodenough *et al.*,[14] the ability of Mo to form molybdyl ions allows a six-fold coordinated Mo(VI) to accept an electron while losing an oxide ligand and, on the other hand, the partner octahedral-site cations (Mn and Mg) are each stable in less
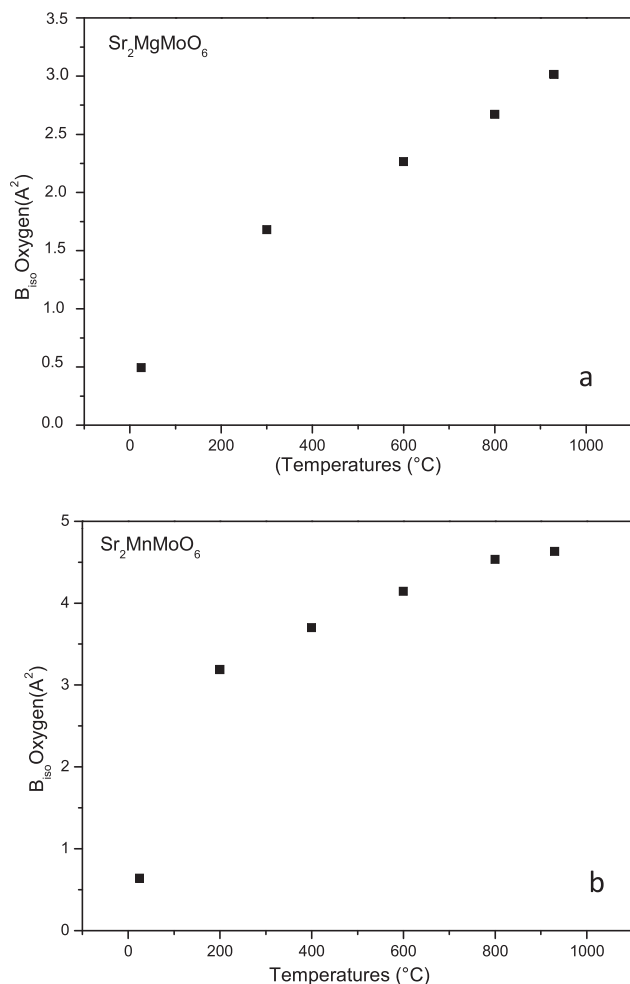
TABLE VI. Interatomic distances (Å) and angles (°) for Sr₂MnMoO₆ from *in situ* NPD data at increasing temperatures. The bold characters indicate the average atomic differences.

T (°C)	25	200	T (°C)	400	T (°C)	600	800	930
Mn–O1 (x2)	2.131(4)	2.130(1)	Mn–O1 (x2)	2.126(8)	Mn–O1 (x12)	2.127(2)	2.130(2)	2.133(2)
Mn–O2 (x2)	2.125(4)	2.017(2)	Mn–O2 (x4)	2.124(7)				
Mn–O3 (x2)	2.131(4)	2.144(1)						
⟨Mn–O⟩	2.129(4)	2.097(2)	**⟨Mn–O⟩**	2.125(8)	**⟨Mn–O⟩**	2.127(2)	2.130(2)	2.133(2)
Mo–O1 (x2)	1.916(4)	1.891(1)	Mo–O1 (x2)	1.904(8)	Mo–O1 (x6)	1.903(2)	1.911(2)	1.915(2)
Mo–O2 (x2)	1.924(4)	2.018(1)	Mo–O2 (x4)	1.912(6)				
Mo–O3 (x2)	1.924(4)	1.904(2)						
⟨Mo–O⟩	1.921(4)	1.937(2)	**⟨Mo–O⟩**	1.908(7)	**⟨Mo–O⟩**	1.903(2)	1.911(2)	1.915(2)
Sr–O1	2.982(4)	2.85(3)	Sr–O1 (x3)	2.842(3)	Sr–O1 (x6)	2.852(1)	2.859(1)	2.864(2)
Sr–O1	2.714(4)	2.82(3)						
Sr–O1	2.551(5)	3.10(4)						
Sr–O2	2.770(7)	2.86(2)	Sr–O2 (x4)	2.994 (5)				
Sr–O2	2.560(7)	2.68(2)	Sr–O2 (x4)	2.707 (4)				
Sr–O2	2.829(8)	3.00(2)						
Sr–O3	2.793(8)	2.89(2)						
Sr–O3	2.803(7)	3.07(2)						
Sr–O3	2.551(7)	2.62(2)						
⟨Sr–O⟩	2.728(6)	2.578(3)	**⟨Sr–O⟩**	2.851(4)	**⟨Sr–O⟩**	2.852(1)	2.859(1)	2.864(2)
Mn–O1–Mo	162.3(2)	169.9(5)	**Mn–O1–Mo**	180.0	Mn–O1–Mo	180.0	180.0	180.0
Mn–O2–Mo	162.4(2)	168.1(6)	**Mn–O2–Mo**	168.4(3)				
Mn–O3–Mo	161.5(2)	164.8(6)						

FIG. 5. Thermal evolution of the equivalent isotropic thermal factors of oxygen atoms for (a) Sr_2MgMoO_6 and (b) Sr_2MnMoO_6.

FIG. 6. Thermal expansion determined by dilatometric measurements in $5\%H_2$-$95\%N_2$ from 35 to $900\,^\circ C$ for (a) Sr_2MgMoO_6 and (b) Sr_2MnMoO_6.

than six-fold oxygen coordination, thus accepting the fast creation and displacement of oxygen vacancies.

CONCLUSIONS

Sr_2MMoO_6 (M = Mg, Mn) double perovskites have recently been described as good candidates for anode materials in SOFCs single cells.[15,16] In the present paper, we have investigated the thermal evolution of their crystal structures that accounts for the observed performance, by *in situ* neutron powder diffraction in the usual working conditions of an anode in SOFCs, in complement with dilatometric analysis. A phase transition of the RT tetragonal I4/m structure to a cubic Fm-3m has been identified below $300\,^\circ C$ for M = Mg, whereas for M = Mn there are two successive phase transitions in the investigated temperature range, from the monoclinic $P2_1/n$ structure stable at RT to tetragonal I4/m (below $400\,^\circ C$) and finally to cubic Fm-3m (below $600\,^\circ C$). There is a progressive reduction of the tilting system, from $a^-b^-c^+$ ($P2_1/n$) to $a^0a^0c^-$ (I4/m) to $a^0a^0a^0$ (Fm-3m). In the high-temperature cubic phase, present at the working temperature of a SOFC, above $600\,^\circ C$, the absence of tilting of the MO_6 (M = Mg, Mn) and MoO_6 octahedra favours the orbital overlap and the electronic conductivity; the lability and high mobility of the oxygen atoms derived from the elevated
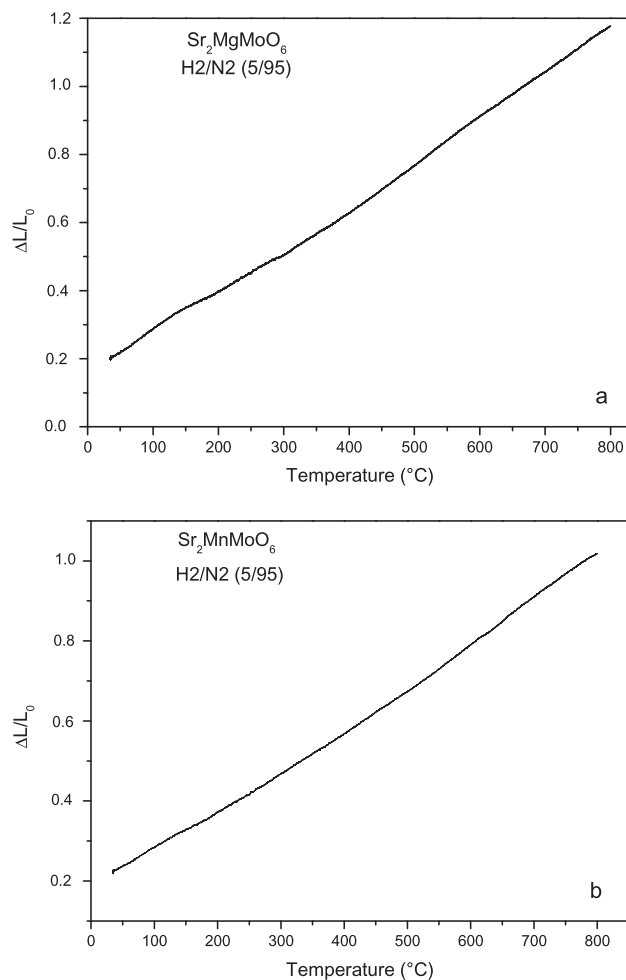
displacement factors in this MIEC oxide account for the excellent performance of these materials as anodes recently described in single fuel cells. The moderated TEC values obtained by dilatometry in the cubic region (12.7×10^{-6} K^{-1} and 13.0×10^{-6} K^{-1}, respectively) are comparable to the values obtained from the refinement of the neutron diffraction data in the heating run and perfectly match those of the usual electrolytes in a SOFC.

ACKNOWLEDGMENTS

[1]Z. Q. Deng, W. S. Yang, W. Liu, and C. S. Chen, J. Solid State Chem. **179**, 362 (2006).
[2]Y. Matsuda, M. Karppinen, Y. Yamazaki, and H. Yamauchi, J. Solid State Chem. **182**, 1713 (2009).
[3]A. Muñoz, J. A. Alonso, M. T. Casais, M. J. Martínez-Lope, and M. T. Fernández-Díaz, J. Phys.: Condens. Matter **14**, 3285 (2002).
[4]D. Marrero-López, J. Peña-Martínez, J. C. Ruiz-Morales, M. C. Martín-Sedeño, and P. Núñez, J. Solid State Chem. **182**, 1027 (2009).

[5]Y. H. Huang, R. I. Dass, J. C. Denyszyn, and J. B. Goodenough, J. Electro-chem. Soc. **153**, A1266 (2006).

[6]H. M. Rietveld, J. Appl. Crystallogr. **2**, 65 (1969).

[7]J. Rodríguez-Carvajal, Physica B **192**, 55 (1993).

[8]C. Bernuy-Lopez, M. Allix, C. A. Bridges, J. B. Claridge, and M. J. Rosseinsky, Chem. Mater. **19**, 1035 (2007).

[9]P. M. Woodward, Acta Crystallogr., Sect. B: Struct. Sci. **53**, 32 (1997).

[10]Z. Wang, Y. Tian, and Y. Li, J. Power Sources **196**, 6104 (2011).

[11]Z. Naiqing, S. Kening, Z. Dewi, and J. De Chang, J. Rare Earths **24**, 90 (2006).

[12]D. Lee, J. H. Han, Y. Chun, R. H. Song, and D. R. Shin, J. Power Sources **166**, 35 (2007).

[13]A. Aguadero, J. A. Alonso, R. Martínez-Coronado, M. J. Martínez-Lope, and M. T. Fernández-Díaz, J. Appl. Phys. **109**, 034907 (2011).

[14]Y. H. Huang, R. I. Dass, Z. L. Xing, and J. B. Goodenough, Science **312**, 254 (2006).

[15]Y. Ji, Y. H. Huang, J. R. Ying, and J. B. Goodenough, Electrochem. Commun. **9**, 1881 (2007).

[16]S. Vasala, M. Lehtimäki, Y. H. Huang, H. Yamauchi, J. B. Goodenough, and M. Karppinen, Solid State Chem. **183**, 1007 (2010).